TENTH AUSTRALASIAN FLUID MECHANICS
CONFERENCE - UNIVERSITY OF MELBOURNE
11-15 DECEMBER 1989

NUMERICAL SIMULATION OF FLOW PAST A CUBE IN A TURBULENT BOUNDARY LAYER

D.A. PATERSON

CSIRO Division of Building Construction and Engineering
P.O. Box 56, Highett, Vic. 3190
AUSTRALIA

ABSTRACT

This paper considers the flow over a surface-mounted cube in several turbulent boundary layers. This flow is simulated on computer by the solution of the Reynolds equation and the continuity equation with the help of a $k-\varepsilon$ model of turbulence. The flow is incompressible and one face of the cube is set perpendicular to the approach flow direction. Computed predictions are compared with experimental measurements.

INTRODUCTION

Flow around a cube in a turbulent boundary layer can be applied to wind flows around structures. Pressures on the structures, velocities at the base of the structures and turbulence in the far wake can be of extreme importance. This flow can also be applied to air flows over trucks, walls and wind tunnel roughness elements; and flows in rivers around obstacles. The flow involves severe pressure gradients, streamline curvature, separation and reattachment, high turbulence levels and some swirl.

THE PRESENT COMPUTATIONAL METHOD

In the computations presented in this paper a steady-state $k-\varepsilon$ model of turbulence is used. The six equations associated with the present version of the $k-\varepsilon$ model of turbulence are:

$$U_j \frac{\partial k}{\partial x_j} = \frac{\partial}{\partial x_j}\left[\frac{\nu_t}{\sigma_k}\frac{\partial k}{\partial x_j}\right] + \nu_t\left[\frac{\partial U_i}{\partial x_j} + \frac{\partial U_j}{\partial x_i}\right]\frac{\partial U_i}{\partial x_j} - \varepsilon$$

$$U_j \frac{\partial \varepsilon}{\partial x_j} = \frac{\partial}{\partial x_j}\left[\frac{\nu_t}{\sigma_\varepsilon}\frac{\partial \varepsilon}{\partial x_j}\right] + c_1 c_\mu k\left[\frac{\partial U_i}{\partial x_j} + \frac{\partial U_j}{\partial x_i}\right]\frac{\partial U_i}{\partial x_j} - c_2\frac{\varepsilon^2}{k}$$

$$U_j \frac{\partial U_i}{\partial x_j} = \frac{\partial}{\partial x_j}\left[\nu_t \frac{\partial U_i}{\partial x_j}\right] - \frac{\partial P}{\partial x_i} \quad i = 1,2,3$$

$$\frac{\partial U_j}{\partial x_j} = 0 \; ; \quad \nu_t = \nu + c_\mu \frac{k^2}{\varepsilon} \; ; \quad P = \frac{\overline{P}}{\rho} + \frac{2}{3}k$$

where U_i is the mean velocity, k is the turbulent kinetic energy, ν_t is the turbulent viscosity, ε is the isotropic dissipation of turbulent kinetic energy, $\overline{P}$ is the mean pressure, ν is the laminar kinematic viscosity and ρ is the fluid density. c_μ, c_1, c_2, σ_k and σ_ε are set to 0.09, 1.44, 1.92, 1.0 and 1.3 respectively. The equations are solved by first decoupling them and then integrating them over appropriate control volumes on a staggered grid. The convection and advection terms in the equations are discretised using the first order hybrid upwinding scheme and the pressure is calculated by the well known SIMPLE method. The grid used in the calculations is a rectangular grid of size 29*13*16 that is finest at the faces of the cube and expands in geometric progression away from these faces.

Dirichlet boundary conditions are used on air/air interfaces. Wall functions for rough wall flow are used on the ground boundary and on the faces of the cube. The algorithm is considered to have converged when the error in all equations – calculated as the sum of the absolute value of the error at each node – is less than 2% of the initial error. The total computation time for the main run reported here is 19 CPU minutes on an IBM 3083E (5 MIPS).

There is a problem, encountered by many researchers, of the underprediction of the size of the recirculation bubbles at the front edges of rectangular obstacles. The usual wall function formulation of boundary conditions for velocity is inadequate for longitudinal velocities adjacent to the windward edges because these velocities are located within the separating shear layer. An *ad hoc* solution is to set these velocities to zero. This solution, here called the recirculation bubble promoter, gives accurate results on coarse grids and tends to the correct limit as the grid is refined.

A COMPARISON OF COMPUTED AND WIND TUNNEL RESULTS

The present calculations are compared with the experimental work by Castro and Robins (1977). In these experiments, the cube height was h = 20 cm and the nominal boundary layer height was 10h. The approach velocity profile could be approximated by a logarithmic law profile with a roughness length of $z_o = 0.02$h. The reference velocity U_r is taken as the velocity in the approach flow at the cube height. The Reynolds number for the flow was in the range 50 000 to 100 000. Some preliminary results have already been published (Paterson 1986, Paterson and Apelt 1986).

The agreement between the present computed results and the measured results is very good. The overall error in the pressure coefficient – calculated from the mean of the absolute values of the errors on the faces of the cube – is 0.045. The computed value of the pressure coefficient ranges from -1.31 to 0.92. The overall error in the present predictions of the longitudinal velocity as a proportion of the reference velocity is also 0.045. The computed value of this velocity ratio ranges from -0.2 to 1.3.

Vertical profiles of the longitudinal velocity fluctuations measured by Castro and Robins are compared with predictions by Vasilic-Melling (1976) and with present predictions in Fig. 1. The fluctuating velocity u' is defined by $u' = \overline{u_1 u_1}^{1/2}$. Despite obvious differences, the agreement between the measured and computed profiles is quite good. The height at which the maximum

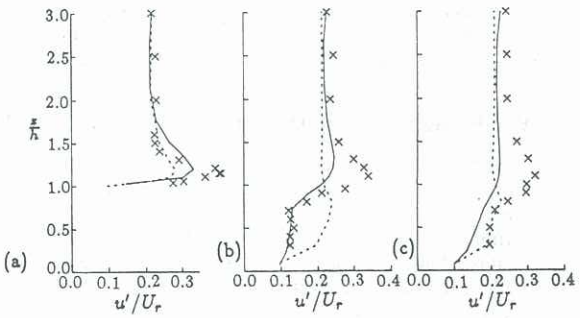

Figure 1 Vertical profiles of longitudinal velocity fluctuations at y/h = 0.12. ——, present computation; -----, from Vasilic-Melling; x, from Castro and Robins: (a) z/h = 0.5; (b) z/h = 1.5; and (c) z/h = 2.5.

velocity fluctuations occur is well predicted by the present computations but not by the computations by Vasilic-Melling. However, the maximum predicted velocity fluctuations are too small and this maximum dies away with distance downstream.

A transverse profile of longitudinal velocity fluctuations measured by Castro and Robins is compared with predictions by Vasilic-Melling in Fig. 2. The magnitude of the velocity fluctuations upstream from the cube in the wind tunnel study is different from that in the computer study and isotropic turbulence is assumed in the approach flow in the computer study, whereas the turbulence measured in the wind tunnel was far from isotropic.

The overall error in the present predictions of the non-dimensionalised longitudinal velocity fluctuations – calculated from the mean of the absolute value of the errors – is 0.045. The magnitudes of the computed fluctuations are less than 0.33. The overall error in the predictions by Vasilic-Melling is 0.055. Although the errors in the computed velocity fluctuations are large compared with the magnitude of those fluctuations, they are small compared with the mean velocities.

MEAN STREAMLINE PATTERNS

Plots of streamlines from mean velocity fields are useful as a tool for visualising three-dimensional flow patterns. These plots should be treated with caution for two reasons. First, the patterns can depend significantly on the interpolation technique used in constructing them, particularly when streamlines pass close to solid surfaces. Second, because of turbulence, actual fluid particles will not follow the mean streamlines and this makes the shapes of the streamlines difficult to confirm by experimental observation. However, the mean streamline patterns presented here have in general been confirmed in a flow visualisation study (Paterson 1986).

Details of the front recirculation region are shown in Fig. 3a. All streamlines in this region turn a full 360° around the swirl axis. This axis passes through the bottom front corners of the cube and through a point 0.5h upstream of the cube and 0.1h above ground level on the symmetry plane. At this grid resolution and with these boundary conditions, there is no indication of the formation of a horseshoe vortex in front of the cube or of a secondary recirculation region near the bottom front edge of the cube. The grid resolution at ground level is 0.055h and at the front of the cube is 0.05h.

Details of the side recirculation region are shown in Fig. 3b. Near the ground the shape of this region is approximately that of a half ellipse. The side recirculation region is much smaller near the top of the cube than near the bottom but the streamlines do not coil more tightly as they rise.

Details of the rear recirculation region are shown in Figs 4a and 4b. The swirl axis lies at an angle of about 25° to the vertical axis. Streamlines that enter the rear recirculation region at the bottom spiral around the swirl axis twice before leaving at the top. As they spiral, they coil more tightly and the orbits become more elliptical.

Details of the top recirculation region are shown in Figs 5a and 5b. This recirculation region is small and streamlines pass forwards and backwards within it many times before leaving. Four streamlines are shown within the region, none are shown leaving. There is a slight spiralling motion away from the plane of symmetry.

FURTHER RESULTS FROM THE MAIN CALCULATION

The results presented in this section are mean velocities near the symmetry plane, turbulence intensities near the symmetry plane, pressure coefficients near the ground and eddy viscosities near the symmetry plane. The plots do not show the whole of the calculation domain. Linear interpolation has been used to get velocity vectors and cubic interpolation to get contours. Figure 6 shows time-averaged velocity vectors on a vertical slice 0.12h from the symmetry plane. In this plot the front, top and rear recirculation regions are clearly shown.

A contour plot of turbulent kinetic energy on a vertical plane 0.12h from the symmetry plane is shown in Fig. 7. This is non-dimensionalised by dividing by the square of the reference velocity. The intensity of turbulence reaches a maximum value above the cube behind the leading edge. In Fig. 1 it was seen that the predicted maximum turbulent kinetic energy is too low. Because of this it is expected that the actual turbulent kinetic energy at a height of about 1.1h will be significantly greater than the predicted values plotted in Fig. 7.

A contour plot of the predicted turbulent viscosity on a vertical plane 0.12h from the symmetry plane is shown in Fig. 8. It has

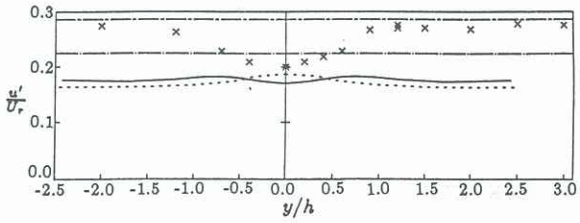

Figure 2 A transverse profile of longitudinal velocity fluctuations at $z/h = 0.5$ and $x/h = 3.5$. ——, present computation; -----, from Vasilic-Melling; x, from Castro and Robins; –·–, present upstream variation; – – –, upstream variation from Castro and Robins.

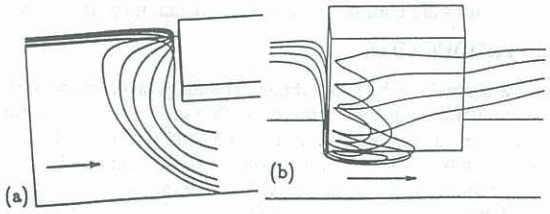

Figure 3 Details of the front and side recirculation regions: (a) a top view of the front recirculation region; and (b) a side view of the side recirculation region.

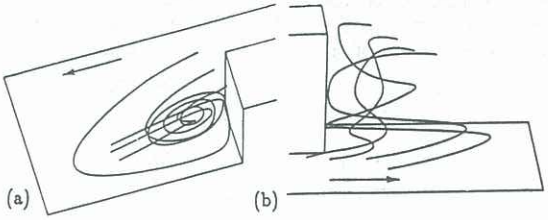

Figure 4 Details of the rear recirculation region: (a) a view down along the swirl axis; and (b) a side view.

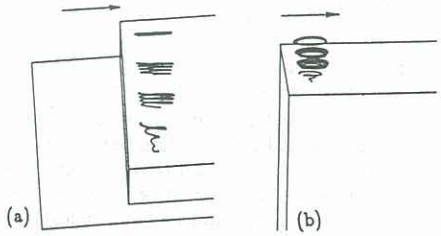

Figure 5 Details of the top recirculation region: (a) an oblique top view; and (b) an oblique side view.

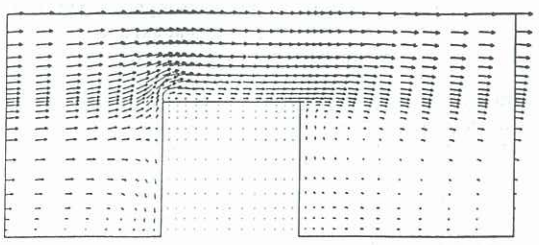

Figure 6 Time-averaged velocity vectors on a vertical slice.

been non-dimensionalised by dividing it by the height of the cube and the reference velocity. In the approach flow the turbulent viscosity increases linearly with height. There is a slight increase in the turbulent viscosity as the flow approaches the cube, followed by a sudden drop near the front face. Directly behind the cube the turbulent viscosity is very small and recovers very slowly.

A contour plot of predicted mean pressure coefficients on a horizontal plane 0.075h above the ground is shown in Fig. 9. In the approach flow the pressure is nearly constant. There is an increase in pressure as the flow approaches the front face of the cube. The pressure drops to a minimum inside the side recirculation region.

DIFFERENT BOUNDARY LAYERS – RESULTS

In this section four radical alterations are made to the boundary layer and the resultant changes in the mean velocities, fluctuating velocities, mean pressures and turbulent viscosities are compared. These four alterations are chosen so that they bracket most practical design situations.

In two alterations the ground roughness is changed. In the main calculation, the ground roughness length is 0.02h. In these two alterations, ground roughness lengths of 0.2h and 0.000005h are used. The first of these corresponds to the situation where the cube is surrounded by roughnesses that are about the same size as the cube itself. The second of these corresponds to smooth wall flow at a Reynolds number of 600 000. A comparison of the resulting velocity profiles is shown in Fig. 10. For each profile there is a nominal zero velocity plane that is above the ground plane a distance equal to the ground roughness length. This arises because the roughness elements surrounding the cube are assumed to be sitting on top of the ground plane. In the present series of calculations the zero velocity plane is taken as the computational boundary.

In the other two alterations the mean velocity profile is retained but the level of turbulence is changed. In these the turbulence intensities are set to match those from the smooth and very rough wall boundary layers described above. This leads to turbulence intensities of 0.088 and 0.677 respectively. The turbulence intensity in the main calculation is 0.274.

A comparison of the four sets of time-averaged velocity vectors on a vertical plane 0.12h from the symmetry plane is given in Fig. 11. Some of the most prominent features of the flow visible in this figure are compared with those in Fig. 6 in Table 1. In general, the shapes and sizes of flow structures vary in the following order: very rough wall flow, high turbulence flow, the main calculation, low turbulence flow, and smooth wall flow. The clearest example of this is the length of the rear recirculation region. One major feature that does not follow the general trend is the length of the front recirculation region.

A comparison of four sets of contours of non-dimensionalised turbulent kinetic energy (NTKE) on a vertical plane 0.12h from the symmetry plane is given in Fig. 12. The plots in this figure can be directly compared with that in Fig. 7. The magnitude of the predicted NTKE is likely to be too small for reasons discussed earlier. For all flows, the maximum NTKE is a distance of about 0.13h above the front of the top face of the cube. The NTKE adjacent to the front and back faces of the cube is small, but is large at a distance of about 0.2h in front of the front face.

A comparison of four sets of contours of non-dimensionalised turbulent viscosity (NTV) on a vertical plane 0.12h from the plane of symmetry is given in Fig. 13. The values in this figure can be compared directly with those in Fig. 8. Upstream of the cube the NTV is roughly proportional to the distance above ground level. Whereas the NTV returns rapidly in the wake to values similar to those upstream in the predictions with a very rough wall boundary layer and with high turbulence flow, this return to normality is extremely slow in the predictions with low turbulence flow and smooth wall flow.

A comparison of four sets of contours of pressure coefficient on a plane 0.055h above the zero velocity plane is given in Fig. 14. The

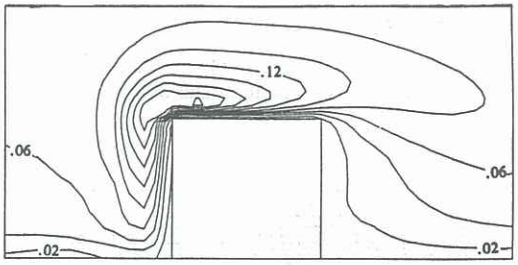

Figure 7 Non-dimensionalised turbulent kinetic energy on a vertical slice.

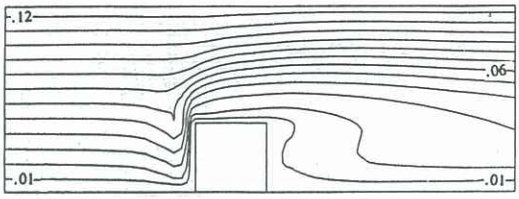

Figure 8 Non-dimensionalised turbulent viscosity on a vertical slice.

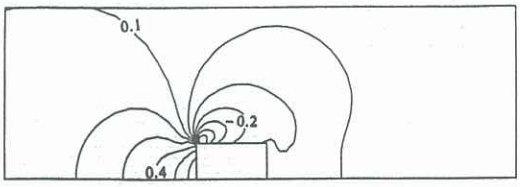

Figure 9 Pressure coefficients near the ground.

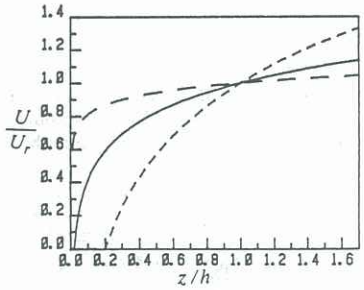

Figure 10 Velocity profiles for different boundary layers. ——, z_0 = 0.02h, main calculation; -----, z_0 = 0.2h, very rough wall flow; – – –, z_0 = 0.000005h, smooth wall flow.

reference pressure coefficient is zero – as opposed to the value of 0.07 used in the production of Fig. 9. The shapes and sizes of most flow structures follow the general trend described above. Changes of this type can be seen in the sideways location of the point of smallest pressure, the magnitude of the smallest pressure, and the magnitude of the pressure in the centre of the back face. The overall pressure pattern for all flows is very similar.

CONCLUSIONS

In the present calculations a steady state $k - \varepsilon$ model of turbulence is used. The total computation time for the main run reported here is 19 CPU minutes at 5 MIPS. The sizes and shapes of recirculation regions are visualised by the use of three-dimensional streamline plots. There is no indication of the formation of a horseshoe vortex in front of the cube. The accuracy of the calculations is considered sufficient for the production of results for use in design and so mean velocities, turbulence intensities, pressure coefficients and eddy viscosities are presented for different boundary layers. It is found that changing the turbulence level in the distant approach flow has effects that are of the same order of magnitude as, but smaller than, the effects of changing both the velocity profile and the turbulence intensity in the approach flow.

REFERENCES

CASTRO, I.P. and ROBINS, A.G. (1977) The flow around a surface mounted cube in uniform and turbulent streams. *J. of Fluid Mech.*, 79, pp. 307-336.

PATERSON, D.A. (1986) Computation of Wind Flows over Three-dimensional Buildings. PhD Thesis, University of Queensland, Brisbane.

PATERSON, D.A. and APELT, C.J. (1986) Computation of wind flows over three-dimensional buildings. *J. of Wind Engin. and Industrial Aerodyn.*, 24, pp. 193-213.

VASILIC-MELLING, D. (1976) Three-dimensional Turbulent Flow Past Rectangular Bluff Bodies. PhD Thesis, Imperial College, London.

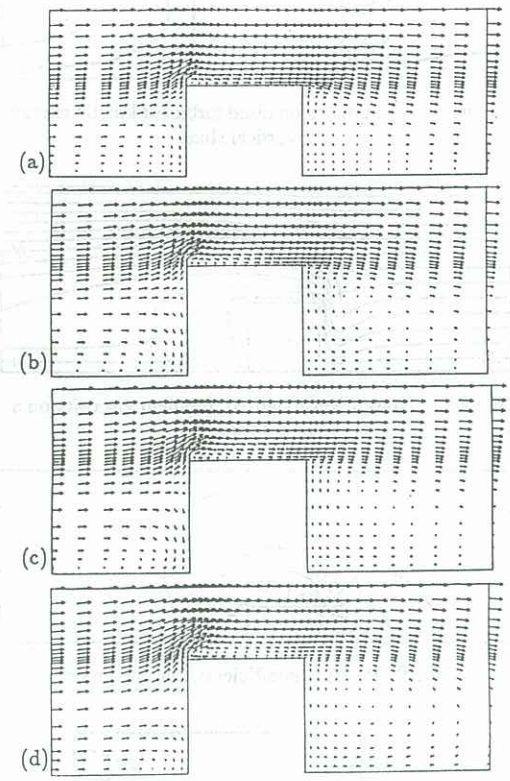

Figure 11 Time-averaged velocity vectors on a vertical slice: (a) very rough wall flow; (b) high turbulence flow; (c) low turbulence flow; and (d) smooth wall flow.

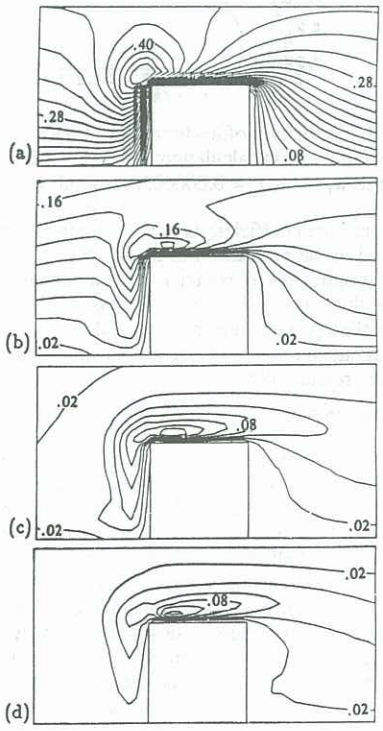

Figure 12 NTKE on a vertical slice: (a) very rough wall flow; (b) high turbulence flow; (c) low turbulence flow; and (d) smooth wall flow.

Table 1 Prominent features of the flow visible in Figs 6 and 11

	Figure				
	11a	11b	6	11c	11d
z_o/h	0.2	0.02	0.02	0.02	0.000005
$\sqrt{k}/U_r$	0.677	0.677	0.274	0.088	0.088
Length rear recirc.	0.9h	1.4h	1.5h	1.7h	2.0h
Length top recirc.	–	0.2h	0.25h	0.3h	0.65h
Height top recirc.	–	0.03h	0.035h	0.04h	0.05h
Height front recirc.	0.85h	0.77h	0.77h	0.77h	0.55h
Ang. flow back corn.	–10°	0	0	0	+15°

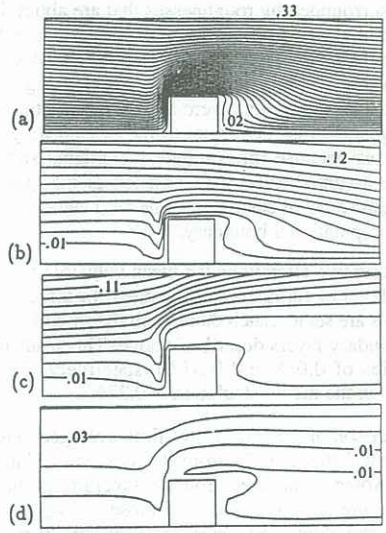

Figure 13 NTV on a vertical slice at: (a) very rough wall flow; (b) high turbulence flow; (c) low turbulence flow; and (d) smooth wall flow.

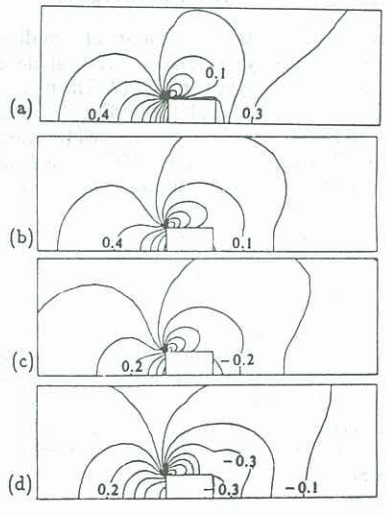

Figure 14 Pressure coefficients near the ground: (a) very rough wall flow; (b) high turbulence flow; (c) low turbulence flow; and (d) smooth wall flow.